


Mass Equilibration and Fluctuations in the Angular Momentum Dependent Dynamics of Heavy Element Synthesis Reactions

T. Tanaka¹, D. J. Hinde¹, M. Dasgupta¹, E. Williams¹, K. Vo-Phuoc¹, C. Simenel^{1,2}, E. C. Simpson¹, D. Y. Jeung¹, I. P. Carter¹, K. J. Cook^{1,*}, N. R. Lobanov¹, D. H. Luong¹, C. Palshetkar¹, D. C. Rafferty¹ and K. Ramachandran^{1,†}

¹Department of Nuclear Physics and Accelerator Applications, Research School of Physics, The Australian National University, Canberra, Australian Capital Territory 2601, Australia

²Department of Fundamental and Theoretical Physics, Research School of Physics, The Australian National University, Canberra, Australian Capital Territory 2601, Australia

 (Received 16 August 2021; revised 12 October 2021; accepted 10 November 2021; published 24 November 2021)

Mass and angle distributions for the $^{52}\text{Cr} + ^{198}\text{Pt}$ and $^{54}\text{Cr} + ^{196}\text{Pt}$ reactions (both forming ^{250}No) were measured and subtracted, giving new information on fast quasifission mass evolution, and the first direct determination of the dependence of sticking times on angular momentum. TDHF calculations showed good agreement with average experimental values, but experimental mass distributions unexpectedly extended to symmetric splits while the peak yield remained close to the initial masses. This implies a strong role of fluctuations in mass division early in the collision, giving insights into the transition from fast energy dissipative deep-inelastic collisions to quasifission.

DOI: [10.1103/PhysRevLett.127.222501](https://doi.org/10.1103/PhysRevLett.127.222501)

Timescales of relaxation processes are important in understanding the dynamics in interactions of many-body quantum systems [1]. Characteristic times in nuclear collisions are $\sim 10^{-21}$ s (zs), thus inaccessible to probes (e.g., lasers) that can be used for atomic systems. However, in nuclear collisions, high angular momentum is typically introduced ($\gtrsim 100\hbar$) resulting in rotation periods of the joined nuclei of ~ 10 zs. This makes rotation angle a good experimental probe to investigate nuclear equilibration time scales [2–4].

This tool has been exploited to probe the dynamics of the nuclear fusion reactions used to synthesize heavy and superheavy elements ($Z \geq 104$ protons). In these collisions of two heavy nuclei, fusion can be suppressed by a factor of $\gtrsim 1000$ [5–7] by the fast nonequilibrium quasifission (QF) process [3,8], as well as deep-inelastic collisions (DIC) [9], reducing superheavy element production cross sections. A fundamental understanding of quasifission, and how it can be minimized, is sought to optimize synthesis of new superheavy isotopes.

Quasifission results in the reseparation of the rotating system into projectilelike and targetlike nuclei after a certain sticking time, during which there is net mass flow towards energetically favorable symmetric mass splits. The correlated distributions of mass and angle is called a mass-angle distribution (MAD) [3,4]. MAD measurements have illuminated many aspects of the physical variables controlling quasifission [2,8,10,11]. Quasifission sticking times range from less than half a rotation (*fast* quasifission [12]) to several rotations (*slow* quasifission). Fast quasifission results in a correlation between mass and angle, giving access to equilibration timescales.

Extracting quantitative information from MADs is limited by two problems. The first is that MADs contain contributions from angular momenta ranging from zero to the maximum that results in capture of the two nuclei. The sticking time t_s determines the rotation angle θ_{rot} while in contact through $\theta_{\text{rot}}(t_s) = L\hbar t_s / \mathcal{I}$, where $L\hbar$ is the angular momentum and \mathcal{I} is the mean moment of inertia. Contributions from a wide range of L make it difficult to map from measured angles to sticking times. The second problem is that in actinide-based reactions, heavy quasifission fragments may themselves undergo fission [3,13]. This could distort the quasifission mass spectrum, affecting conclusions regarding equilibration.

In this Letter, we overcome both these problems, giving the first direct experimental measurement of the angular momentum dependence of the quasifission sticking time, and a new description of mass evolution in fast quasifission. MADs were measured for the $^{52}\text{Cr} + ^{198}\text{Pt}$ and $^{54}\text{Cr} + ^{196}\text{Pt}$ reactions, both forming ^{250}No , at four excitation energies E_x . The different initial neutron numbers should rapidly equalize through transfer reactions [1,14,15]. The key difference is the different binding energies of the colliding nuclei. For the same E_x after contact, this results in L distributions with different maximum L values for the two reactions. Subtracting the MAD with the lower maximum L reveals for the first time the MAD (and thus the dynamics) for the much narrower “difference” angular momentum distribution. Using $^{196,198}\text{Pt}$ nuclei eliminates the possibility of sequential fission distorting the binary mass spectra, since their fission barriers are 23–25 MeV [16], making the probability of sequential fission negligible. Being neither spherical magic nuclei, nor having

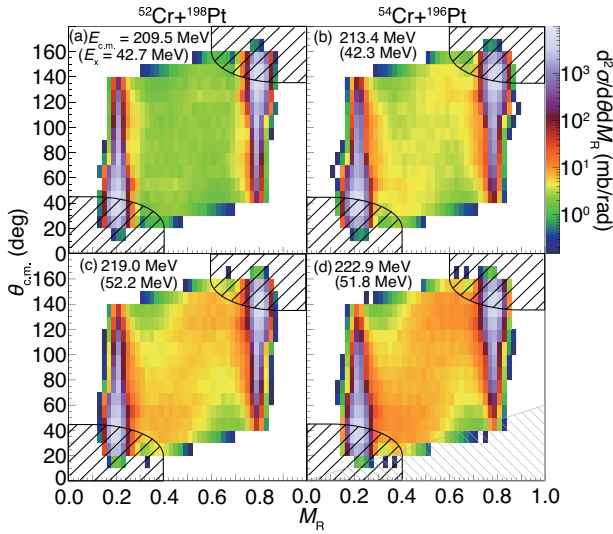


FIG. 1. Measured pairs of MADs (a),(b) and (c),(d) for the indicated reactions leading to similar E_x in ^{250}No . Black hatched regions indicate reduced detector efficiency due to low heavy fragment pulse heights. The gray hatched region in (d) indicates little or no detector coverage, also applicable at mirrored angles [26], and to all MADs.

large static deformations, these effects on the reaction dynamics are minimized [8,10,14].

The experiments were performed at the Heavy Ion Accelerator Facility of the Australian National University. Pulsed beams [17,18] of $^{52,54}\text{Cr}$ (FWHM ~ 700 ps) were provided by the 14UD electrostatic accelerator [19] and superconducting Linac [20]. They bombarded isotopically enriched targets of $^{196,198}\text{Pt}$ of thickness 190 and 40 $\mu\text{g}/\text{cm}^2$, respectively, on 20 $\mu\text{g}/\text{cm}^2$ carbon backings, at near-barrier energies (see Supplemental Material [21]).

Binary reaction products were detected in coincidence using two large-area, position-sensitive multiwire proportional counters, whose normals (18 cm from the target) were centered at scattering angles of 45° and 90° (see Fig. 1 of Ref. [24]).

Time-of-flight and position information from the detectors provided the fragment velocity vectors, which were analyzed by the kinematic coincidence technique [3,25,26]. This gave the mass ratio $M_R = m_1/(m_1 + m_2)$ (where m_1 and m_2 are the masses of the reaction product), the total kinetic energy (TKE), and the center-of-mass scattering angle $\theta_{\text{c.m.}}$. Representative MADs are shown in Fig. 1. Consistent with systematics [26,27], they are dominated by fast quasifission, with no clear vertical band centred at mass-symmetry from slow fissionlike processes.

Quantitative information from the subtracted MADs were obtained by (i) determine the angular momentum distributions for the fast quasifission events; (ii) use these to obtain the angular momentum distributions associated with the subtracted MADs; (iii) with trial functions describing $M_R(t_s)$ (the evolution of M_R with sticking time), fit the

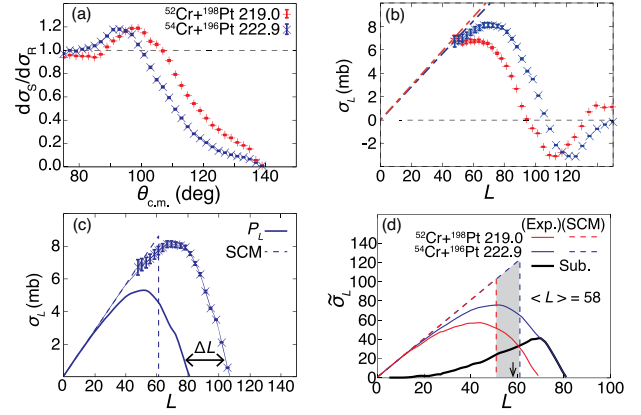


FIG. 2. (a) Scattering cross section relative to the Rutherford cross section $d\sigma_S/d\sigma_R$ with respect to $\theta_{\text{c.m.}}$. (b) Deduced cross sections σ_L for each angular momentum, from $d\sigma_S/d\sigma_R$. (c) Total (symbols) and quasifission partial cross sections σ_L vs L from P_L values shifted by ΔL (see text), and the sharp-cutoff model (SCM). (d) Experimental and SCM reduced cross sections $\tilde{\sigma}_L = \sigma_L/\pi\lambda^2$ vs L for the primary reactions (thin lines). The experimental difference distribution is shown by the thick line. The $\langle L \rangle$, indicated by the arrow, is close to the $\text{SCM}\langle L \rangle$.

subtracted MADs, and determine both $M_R(t_s)$ and the dependence of t_s on angular momentum.

Step (i) is problematic, since measured quasifission cross sections are significantly smaller than standard capture models [9,13]. Therefore a novel approach described below, using only experimental data, was developed to determine empirically the L distribution (σ_L^{QF}) of the quasifission cross section $\sigma_{\text{QF}} = \sum \sigma_L^{\text{QF}}$. First, σ_{QF} was determined in the range $0.28 < M_R < 0.72$ (to eliminate contamination by quasielastic events). The experimental angular coverage $\theta_{\text{c.m.}} = 40^\circ\text{--}140^\circ$ was extrapolated to $0^\circ, 180^\circ$ using the best fits from quasifission simulations [2,13].

The σ_L^{QF} are defined in terms of a probability P_L^{QF} that each L value results in capture followed by quasifission:

$$\sigma_L^{\text{QF}} = \pi\lambda^2(2L + 1)P_L^{\text{QF}}, \quad (1)$$

where λ is the reduced de-Broglie wavelength. P_L^{QF} is expected to be ~ 1 for low L , and ~ 0 at large L , giving \sim triangular distributions of σ_L^{QF} [Fig. 2(c)].

From σ_{QF} alone, the mean angular momentum can be estimated, but here two L distributions must be subtracted, so knowledge of the *shape* of the L distributions at high L is desirable. This information is sourced from the scattering angular distributions. Assuming scattering follows Rutherford trajectories, the ratio of scattering cross section to the Rutherford cross section $d\sigma_S/d\sigma_R(\theta_{\text{c.m.}})$ can be written $d\sigma_S/d\sigma_R(\theta_{\text{c.m.}}) = [1 - T(\theta_{\text{c.m.}})]$, where $T(\theta_{\text{c.m.}})$ is the probability at $\theta_{\text{c.m.}}$ that flux is removed from the Rutherford trajectory by complex reactions such as quasifission and DIC.

The $d\sigma_S/d\sigma_R(\theta_{c.m.})$ for scattering ($M_R < 0.28$) for the two reactions populating ^{250}No at $E_x \sim 52$ MeV are presented in Fig. 2(a), showing the expected falloff at backward angles. The partial cross sections σ_L for complex reactions were obtained by mapping from $T(\theta_{c.m.})$ to T_L (the equivalent probability at L) and substituting for P_L^{QF} in Eq. (1).

Mapping was achieved using the Coulomb deflection function [28,29], giving $L = (D/2\lambda) \cot(\theta_{c.m.}/2)$, where D is the distance of closest approach in a head-on collision. Distributions of σ_L are shown in Fig. 2(b), displaying the expected smoothed triangular shape, but also a negative component, associated with $d\sigma_S/d\sigma_R > 1$ [Fig. 2(a)]. This feature likely results from DIC trajectories (with $M_R < 0.28$) deflected to more forward angles, resulting in higher-than-Rutherford yields. The positive values of the experimental σ_L [Fig. 2(c)] were adopted and attributed to both DIC + QF reactions. To extract the quasifission σ_L^{QF} using Eq. (1), we recognize that DIC is expected at the highest L values [29], so we take $P_{(L-\Delta L)}^{\text{QF}} = T_L$, where ΔL is a fixed L offset chosen such that $\sigma_{\text{QF}} = \pi\lambda^2 \Sigma(2L+1)P_L^{\text{QF}}$ matches experimental cross sections. Figure 2(c) shows ΔL and σ_L^{QF} (solid line).

To subtract L distributions for reactions with different λ , dimensionless reduced cross sections [6,30] $\tilde{\sigma}_L = \sigma_L/\pi\lambda^2$ must be used [Fig. 2(d), solid lines]. The experimental difference L distribution (thick line with $\langle L \rangle$ indicated) is responsible for the difference in the MADs for the two reactions. A sharp-cutoff model (SCM) gives different distributions (dashed lines), but very similar $\langle L \rangle$.

To obtain the MADs associated with the difference L distributions, the measured MADs for the two reactions, normalized by the corresponding $\pi\lambda^2$, were subtracted. Two of the four subtracted MADs are shown in Figs. 3(a) and 3(b). They show (i) that for all $\theta_{c.m.}$, the quasifission yield initially falls monotonically towards mass symmetry, and (ii) that with higher $\langle L \rangle$, the quasifission distribution moves to more forward angles, as expected.

If the subtracted MADs resulted from a single L value, direct mapping from $\theta_{c.m.}$ to sticking time could be achieved. However, since MAD subtraction results in a range of L values [Fig. 2(d)], quantitative analysis requires a quasifission simulation, described below.

The $\theta_{c.m.}$ of fast quasifission events were calculated following Töke *et al.* [3,4], as implemented in Refs. [2,11,13,26,31]. The ingredients are incoming Coulomb trajectories up to contact θ_{in} , rotation through angles θ_{rot} while in contact, and outgoing Coulomb trajectories of the quasifission fragments θ_{out} [26]. The measured angle $\theta_{c.m.} = \pi - \theta_{\text{in}} - \theta_{\text{rot}} - \theta_{\text{out}}$ [3,26]. As well as the L values (from experiment), calculation of θ_{rot} during t_s requires the average moment of inertia \mathcal{I} . From TDHF calculations [32,33] for Cr + Pt, $\mathcal{I} = 2.02 \times 10^{-53}$ kg m² was adopted, 2.04 times the spherical value [11].

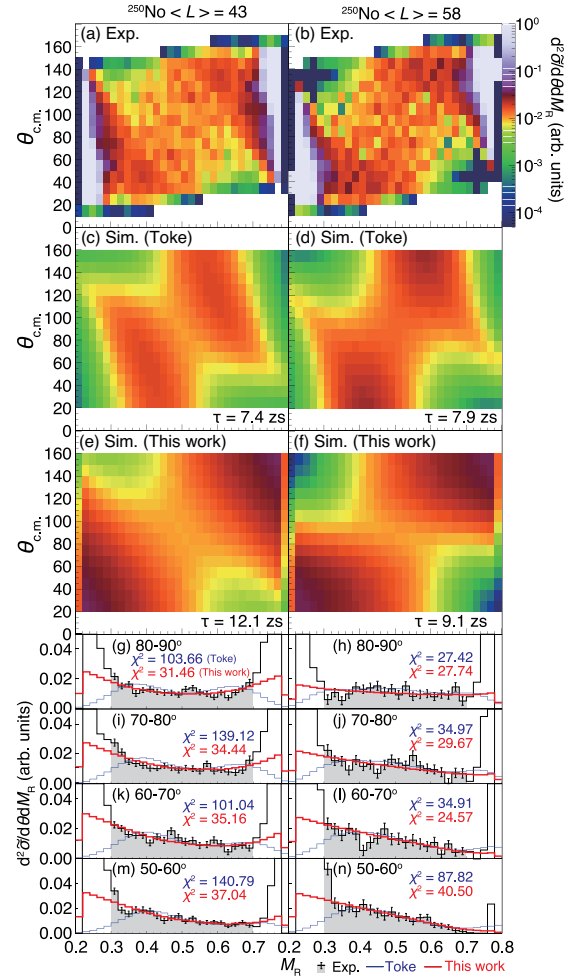


FIG. 3. Experimental subtracted MADs are shown in (a) and (b) for the indicated $\langle L \rangle$. Corresponding best-fit simulations from the picture of Töke are in (c),(d), and from the mass evolution picture of this work in (e),(f). Mean sticking times τ are given. Projected experimental (black) and simulated M_R spectra (thin blue and thick red histograms) for the indicated c.m. angle ranges are given in (g)–(n), with the total χ^2 values indicated in blue (Töke) and red (this work).

The second variable in the MAD is the fragment mass-ratio M_R at scission. In the simulation, the first trial function for $M_R(t_s)$ came from the parametrization of Töke *et al.* [3,4,26], where the mean mass-split approaches 0.5 asymptotically with increasing time [see Fig. 4(c)]. A Gaussian distribution of M_R was assumed [2,11,26], widening as the system approaches symmetry [see Fig. 4(a)].

Using the standard [3] mass equilibration time constant of 5.3 zs following an initial delay of 1 zs [4], the four subtracted MADs were individually fitted by varying the mean τ and standard deviation σ_τ of the assumed Gaussian distribution of sticking times t_s . The best fitting MADs are presented in Figs. 3(c) and 3(d), for the values of τ indicated. Projected experimental and simulated (blue histograms) M_R distributions for 10° slices in $\theta_{c.m.}$ are

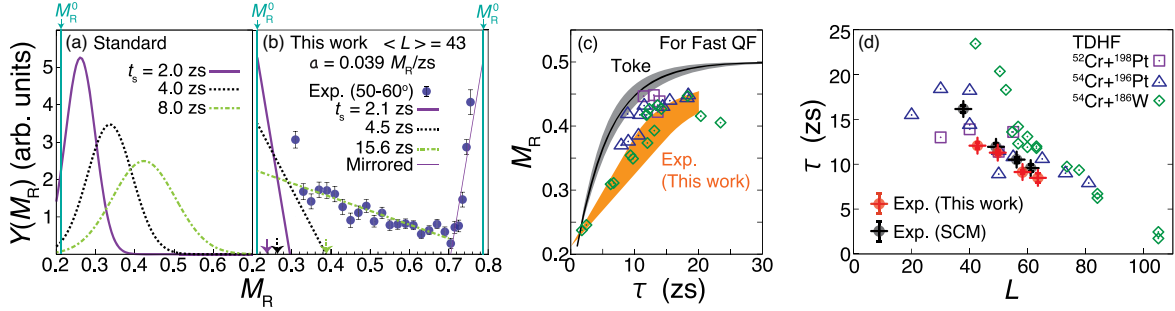


FIG. 4. (a) M_R distributions as a function of t_s in previous simulations of quasifission. (b) Experimental M_R distribution showing projectilelike (green dash-dotted line) and targetlike (purple thin line) components, the lines representing the new description of time-dependent M_R distributions for three values of t_s . Bottom arrows indicate the mean M_R for each t_s . (c) mean M_R vs mean sticking time τ from the present experimental results and for the prescription of Ref. [3], together with results of TDHF calculations. (d) Mean sticking time vs mean angular momentum from the current experiments, for L distributions from experiment (red points) and the sharp-cutoff model (black points). Results of TDHF calculations at single L values are shown for the indicated reactions.

shown in Fig. 3(g)–3(n). The fit regions are shaded gray. The simulation gives too little yield close to the initial mass ratio of the projectile and target M_R^0 , with total χ^2 for each spectrum averaging 84.

Experimentally, a monotonic fall in yield from the projectile and target masses towards mass symmetry was observed; see Fig. 4(b). This prompted a new trial function describing mass evolution in fast quasifission. A rapid linear fall in yield $Y(M_R)$ from M_R^0 is assumed for small t_s , with slope decreasing as t_s increases. This is shown in Fig. 4(b), and described by

$$Y(M_R) = A \left[1 - \frac{M_R - M_R^0}{at_s} \right]. \quad (2)$$

Here at_s is the slope parameter, taken as depending linearly on t_s , and A provides normalization.

To obtain the best fit to each subtracted MAD, the parameter a , the mean sticking time τ , and its Gaussian standard deviation σ_τ (which determine the angular distribution) were varied freely. The optimum simulated MADs are shown in Fig. 3(e) and 3(f), and the M_R spectra in Fig. 3(g)–3(n) (red histograms). The agreement is improved, with the average χ^2 for each spectrum falling from 84 to 33.

From the fits to the four subtracted MADs, four values of τ , σ_τ , and a were obtained. The a values ranged from 0.039 to 0.059 zs^{-1} , averaging 0.047 zs^{-1} . From each a value, the change in mean mass ratio $\langle M_R \rangle$ with time was evaluated using Eq. (2). The orange band in Fig. 4(c) covers the full range of a values. The form resembles that of Töke (gray band), but $\langle M_R \rangle$ approaches 0.5 more slowly, as found in previous fast quasifission analyses [11,31]. Although this new mass evolution picture describes *fast* quasifission in these reactions, it cannot describe any *slow* quasifission component, since it cannot generate the peak in $Y(M_R)$ observed [12,26,34] close to $M_R \sim 0.5$.

Sticking times and final M_R values from the TDHF calculations carried out in this work are also shown in Fig. 4(c), together with previous calculations for $^{54}\text{Cr} + ^{186}\text{W}$ [1,27,32]. They lie closer to the new experimental values than to the Toke ansatz.

The surprising conclusion is that fast quasifission M_R distributions extend beyond mass-symmetry while still peaked near M_R^0 , as seen in Fig. 4(b). Many quasifission M_R distributions have been measured for reactions with actinide nuclei [3,4,10,12,35–37], which show little quasifission yield near M_R^0 , suggesting M_R distributions peak around the mean M_R . The present fast quasifission results indicate that this need not be the case, and that theoretical predictions of $\langle M_R \rangle$, such as from TDHF, may not necessarily represent the outcome with the highest $Y(M_R)$.

We now turn to the original goal of this work, to extract the dependence of the fast quasifission mean sticking time on angular momentum. Figure 4(d) shows (red points) the centroids τ of the assumed Gaussian sticking time distributions extracted from the experimental data, plotted at the mean angular momenta $\langle L \rangle$ of the difference L distributions. The time decreases with angular momentum, as might be expected. The robustness of our method is demonstrated by the small sensitivity to the shape of the quasifission L distributions. Even fitting the experimental subtracted MADs using the L distributions from the extreme sharp-cutoff model [see Fig. 2(d)] gives a very similar trend, as shown by the black points in Fig. 4(d). The TDHF calculated sticking times [Fig. 4(c)] are also plotted as a function of the input L value. The agreement of both the absolute sticking times and their dependence on L is remarkable. This dependence of τ on L supports our assumption that DIC occurs at the highest L . It also indicates that the lowest L are most likely to result in slow quasifission, and by implication in fusion.

DIC is considered to be the “energy damping mode” [3], with peak mass yield close to M_R^0 , and angular distributions around the grazing angle [38]. In contrast, quasifission is

typically fully damped in kinetic energy, but with significant angular rotation and mass evolution towards symmetry. From experimental data for reactions of ^{54}Cr with ^{208}Pb (doubly magic), it was proposed [9] that DIC and quasifission form a continuum. The evidence is even stronger in these Cr + Pt reactions, where M_R distributions extend with significant probability beyond mass symmetry while still peaked near M_R^0 , and thus before the *peak* yield drifts significantly from M_R^0 towards symmetry. This behavior appears to be intermediate between DIC and slow quasifission, suggesting a strong role of fluctuations, growing with time during the reaction, in contrast with the standard quasifission ansatz of Ref. [3]. Further investigations are needed.

In conclusion, mass-angle distributions for the $^{52}\text{Cr} + ^{198}\text{Pt}$ and $^{54}\text{Cr} + ^{196}\text{Pt}$ reactions (both forming ^{250}No) were measured at selected energies. A new experimental method, involving subtraction of two measured MADs, has enabled the first direct determination of the dependence of the fast quasifission sticking time on angular momentum $L\hbar$. The results are consistent with a transition from slow quasifission (and fusion) at the lowest L , through fast quasifission at intermediate L to DIC at the highest L . TDHF calculations are in good agreement.

The observed *fast* quasifission mass evolution is inconsistent with the standard picture of the peak mass yield drifting towards symmetric splits. Surprisingly, the mass distributions can extend to symmetric splits even though the peak yield remains close to the entrance channel masses. This implies a very strong role for fluctuations in determining fissionlike mass partitions during the first 10 zs after contact.

The authors acknowledge the Australian Research Council for support through Discovery Grants No. DP200100601, No. DP190100256, No. DP190101442, No. DP170102318, and No. DE140100784. Financial support from the National Collaborative Research Infrastructure Strategy (NCRIS) Heavy Ion Accelerators (HIA) capability for operation of the Heavy Ion Accelerator Facility is acknowledged. The authors thank T. Kibédi for his key role in operation of the Linac.

*Present address: Facility for Rare Isotope Beams and Department of Physics and Astronomy, Michigan State University, East Lansing, Michigan 48824, USA.

†Permanent address: Nuclear Physics Division, Bhabha Atomic Research Centre, Mumbai 400085, India.

- [1] C. Simenel, K. Godbey, and A. S. Umar, *Phys. Rev. Lett.* **124**, 212504 (2020).
- [2] R. du Rietz, D. J. Hinde, M. Dasgupta, R. G. Thomas, L. R. Gasques, M. Evers, N. Lobanov, and A. Wakhle, *Phys. Rev. Lett.* **106**, 052701 (2011).
- [3] J. Toke, R. Bock, G. X. Dai, A. Gobbi, S. Gralla, K. D. Hildenbrand, J. Kuzminski, W. F. J. Muller, A. Olmi, H. Stelzer, B. B. Back, and S. Bjornholm, *Nucl. Phys.* **A440**, 327 (1985).
- [4] W. Q. Shen, J. Albinski, A. Gobbi, S. Gralla, K. D. Hildenbrand, N. Herrmann, J. Kuzminski, W. F. J. Muller, H. Stelzer, J. Toke, B. B. Back, S. Bjornholm, and S. P. Sdrensen, *Phys. Rev. C* **36**, 115 (1987).
- [5] G. G. Adamian, N. V. Antonenko, and W. Scheid, *Nucl. Phys.* **A678**, 24 (2000).
- [6] D. J. Hinde, M. Dasgupta, and A. Mukherjee, *Phys. Rev. Lett.* **89**, 282701 (2002).
- [7] E. M. Kozulin, G. N. Knyazheva, K. V. Novikov, I. M. Itkis, M. G. Itkis, S. N. Dmitriev, Yu. Ts. Oganessian, A. A. Bogachev, N. I. Kozulina, I. Harca, W. H. Trzaska, and T. K. Ghosh, *Phys. Rev. C* **94**, 054613 (2016).
- [8] D. J. Hinde, M. Dasgupta, and E. C. Simpson, *Prog. Part. Nucl. Phys.* **118**, 103856 (2021).
- [9] K. Banerjee *et al.*, *Phys. Rev. Lett.* **122**, 232503 (2019).
- [10] D. J. Hinde, R. du Rietz, M. Dasgupta, R. G. Thomas, and L. R. Gasques, *Phys. Rev. Lett.* **101**, 092701 (2008).
- [11] E. Prasad, A. Wakhle, D. J. Hinde, E. Williams, M. Dasgupta, M. Evers, D. H. Luong, G. Mohanto, C. Simenel, and K. Vo-Phuoc, *Phys. Rev. C* **93**, 024607 (2016).
- [12] D. J. Hinde, D. Y. Jeung, E. Prasad, A. Wakhle, M. Dasgupta, M. Evers, D. H. Luong, R. du Rietz, C. Simenel, E. C. Simpson, and E. Williams, *Phys. Rev. C* **97**, 024616 (2018).
- [13] D. Y. Jeung, D. J. Hinde, E. Williams, M. Dasgupta, E. C. Simpson, R. du Rietz, D. H. Luong, R. Rafiei, M. Evers, I. P. Carter, K. Ramachandran, C. Palshetkar, D. C. Rafferty, C. Simenel, and A. Wakhle, *Phys. Rev. C* **103**, 034603 (2021).
- [14] C. Simenel, D. J. Hinde, R. du Rietz, M. Dasgupta, M. Evers, C. J. Lin, D. H. Luong, and A. Wakhle, *Phys. Lett. B* **710**, 607 (2012).
- [15] K. Sekizawa and K. Yabana, *Phys. Rev. C* **88**, 014614 (2013); **93**, 029902(E) (2016).
- [16] P. Möller, A. J. Sierk, T. Ichikawa, A. Iwamoto, and M. Mumpower, *Phys. Rev. C* **91**, 024310 (2015).
- [17] N. R. Lobanov, P. Linardakis, and D. Tempra, *Nucl. Instrum. Methods Phys. Res., Sect. B* **499**, 133 (2021).
- [18] N. R. Lobanov, P. Linardakis, and D. Tempra, *Nucl. Instrum. Methods Phys. Res., Sect. B* **499**, 142 (2021).
- [19] T. R. Ophel, J. S. Harrison, J. O. Newton, R. H. Spear, E. W. Titterton, and D. C. Weisser, *Nucl. Instrum. Methods* **122**, 227 (1974).
- [20] T. Kibédi, D. C. Weisser, N. Lobanov, R. B. Turkentine, A. G. Muirhead, and D. J. Anderson, *Nucl. Instrum. Methods Phys. Res., Sect. A* **382**, 167 (1996).
- [21] See Supplemental Material at <http://link.aps.org/supplemental/10.1103/PhysRevLett.127.222501> for the detailed experimental informations, which includes Refs. [22–23].
- [22] D. J. Hinde, D. Hilscher, H. Rossner, B. Gebauer, M. Lehmann, and M. Wilpert, *Phys. Rev. C* **45**, 1229 (1992).
- [23] V. E. Viola, K. Kwiatkowski, and M. Walker, *Phys. Rev. C* **31**, 1550 (1985).
- [24] K. Hammerton, D. J. Morrissey, Z. Kohley, D. J. Hinde, M. Dasgupta, A. Wakhle, E. Williams, I. P. Carter, K. J. Cook, J. Greene, D. Y. Jeung, D. H. Luong, S. D. McNeil, C. Palshetkar, D. C. Rafferty, C. Simenel, and K. Stiefel, *Phys. Rev. C* **99**, 054621 (2019).

- [25] D. J. Hinde, M. Dasgupta, J. R. Leigh, J. C. Mein, C. R. Morton, J. O. Newton, and H. Timmers, *Phys. Rev. C* **53**, 1290 (1996).
- [26] R. du Rietz, E. Williams, D. J. Hinde, M. Dasgupta, M. Evers, C. J. Lin, D. H. Luong, C. Simenel, and A. Wakhle, *Phys. Rev. C* **88**, 054618 (2013).
- [27] K. Hammerton, Z. Kohley, D. J. Hinde, M. Dasgupta, A. Wakhle, E. Williams, V. E. Oberacker, A. S. Umar, I. P. Carter, K. J. Cook, J. Greene, D. Y. Jeung, D. H. Luong, S. D. McNeil, C. S. Palshetkar, D. C. Rafferty, C. Simenel, and K. Stiefel, *Phys. Rev. C* **91**, 041602(R) (2015).
- [28] E. Rutherford, *Philos. Mag. Ser. 6* **21**, 669 (1911).
- [29] R. Bass, *Nucl. Phys. A* **231**, 45 (1974); *Nuclear Reactions with Heavy Ions* (Springer, New York, 1980).
- [30] A. Berriman, D. J. Hinde, M. Dasgupta, C. Morton, R. Butt, and J. Newton, *Nature (London)* **413**, 144 (2001).
- [31] E. Prasad, D. J. Hinde, E. Williams, M. Dasgupta, I. P. Carter, K. J. Cook, D. Y. Jeung, D. H. Luong, C. S. Palshetkar, D. C. Rafferty, K. Ramachandran, C. Simenel, and A. Wakhle, *Phys. Rev. C* **96**, 034608 (2017).
- [32] K. Vo-Phuoc, Doctoral dissertation, The Australian National University, 2018.
- [33] C. Simenel and A. S. Umar, *Prog. Part. Nucl. Phys.* **103**, 19 (2018).
- [34] J. Khuyagbaatar, D. J. Hinde, I. P. Carter, M. Dasgupta, Ch. E. Düllmann, M. Evers, D. H. Luong, R. du Rietz, A. Wakhle, E. Williams, and A. Yakushev, *Phys. Rev. C* **91**, 054608 (2015).
- [35] A. Wakhle, C. Simenel, D. J. Hinde, M. Dasgupta, M. Evers, D. H. Luong, R. du Rietz, and E. Williams, *Phys. Rev. Lett.* **113**, 182502 (2014).
- [36] H. M. Albers, J. Khuyagbaatar, D. J. Hinde, I. P. Carter, K. J. Cook, M. Dasgupta *et al.*, *Phys. Lett. B* **808**, 135626 (2020).
- [37] K. Nishio, H. Ikezoe, S. Mitsuoka, I. Nishinaka, Y. Nagame, Y. Watanabe, T. Ohtsuki, K. Hirose, and S. Hofmann, *Phys. Rev. C* **77**, 064607 (2008).
- [38] E. M. Kozulin, E. Vardaci, G. N. Knyazheva, A. A. Bogachev, S. N. Dmitriev, I. M. Itkis, M. G. Itkis, A. G. Knyazev, T. A. Loktev, K. V. Novikov *et al.*, *Phys. Rev. C* **86**, 044611 (2012).